# Anemometer Measurements of Velocity and Density in Projectile Wakes

JAY FOX* AND HARALD RUNGALDIER†
*TRW Systems Group, Redondo Beach, Calif.*

**Mean and fluctuating wake properties including both velocity and density (or inverse temperature in the constant-pressure far wake) were measured with hot-film and cooled-film anemometers. The projectiles were half-inch spheres at 6 kfps, 0.38-in. slender cones at 6.5 kfps, and 0.22-in. blunt bullets at 4 kfps. Simulated altitude was used during many tests, data being analyzed from $10^2$ to $10^5$ diam behind the projectiles. The measurements of velocity, density, and space correlation length agreed with the analytical predictions of these quantities using the Lees-Hromas-Webb theory. For the sphere wakes, both space and time correlation had a distinctive character at low $X/D$ which showed that the structure of the temperature or density fluctuations was of larger scale than the structure of the velocity fluctuations; both scales agreed at great $X/D$. In the comparisons with other data, good agreement was found with localized measurements obtained by probes, but less agreement was found with measurements obtained by optical methods.**

## Nomenclature

$A$ = base area of body or projectile
$C_D$ = drag coefficient
$C_{gh}$ = correlation coefficient
$c_p$ = specific heat at constant pressure
$D$ = diameter of body or projectile
$g,h$ = digitized anemometer data
$h$ = enthalpy
$M$ = Mach number
$P$ = power spectral density
$q$ = heat loss from anemometer probe
$R$ = covariance or gas constant
$t,\Delta t$ = time, delay time
$T,\Delta T$ = temperature, temperature difference
$U$ = velocity
$X$ = distance behind body or projectile
$\Delta X$ = probe separation distance
$\gamma$ = specific heat ratio
$\theta$ = time correlation integral scale
$\rho$ = mass density
$\Lambda$ = space correlation length scale

***Subscripts and superscripts***

$\langle\ \rangle$ = average
$(\ )'$ = fluctuation
$(\ )_\infty$ = projectile

## 1. Introduction

MOST of the important features of hypersonic wakes are contained in the $X/D$ range of $10^2$–$10^5$, this $X/D$ range being covered by the new anemometer measurements of projectile wakes. For $X/D$ less than about $10^3$, the inviscid drag deposited by the bow shock is being swallowed by the turbulent wake. In the intermediate range of $X/D$ from $10^3$ to $10^4$, blunt body wakes at high Mach number are hot enough after the inviscid wake is swallowed to produce a rapidly decaying wake velocity as they cool down. Lower Mach number wakes produce less of this effect, the velocity rapidly approaching the asymptotic $X^{-2/3}$ slope. High Mach number blunt-body wakes, on the other hand, may require $X/D$ values as large as $10^5$ to achieve this slope.

The new anemometer results cover a large range of $X/D$ that has been seldom measured by probes. Earlier measurements[1,2] were at lower $X/D$ where the off-axis effects on the measurements were greater, and thus the uncertainties in the axis values were greater. The present measurements are in the region of wake where all the wake velocities coalesce, when scaled as $U/U_\infty$ against $X/(C_DA)^{1/2}$, to the value predicted by the Lees-Hromas-Webb (LHW) computations.[3–7] Thus, these measurements have been effective in the validation of the LHW theory.

Previous measurements of density and density fluctuations have used optical techniques (schlieren, interferometer) that integrate across the wake,[8,9] or focusing optical systems.[10,11] In contrast, the anemometer measures local properties with a small sensor; there is none of the path dependence that accompanies optical systems. The sensitivity of the anemometer to temperature fluctuations is convertible into density fluctuations in the far wake, which has constant pressure. The preliminary fluctuation intensity measurements obtained with anemometers are comparable with previous measurements in low Mach number wakes.[12–14]

The scale and spectrum of the turbulence is readily studied with anemometers using both auto-correlation and cross-correlation techniques.[15,16] Similar results are produced by the two methods when Taylor's hypothesis is used for converting the time correlation scale into space correlation length or scale.

## 2. Experimental Techniques

The experimental arrangement is shown in Fig. 1. Two anemometer probes were placed adjacent to the projectile path but with sufficient clearance to assure survival of the hot-film or cooled-film sensors. The cylindrical sensors of 0.001 and 0.006-in. diam, respectively, were aligned, as shown in Fig. 1, so as to be sensitive to axial and radial velocity fluctuations of the growing wake. Both probes

Received August 4, 1969; revision received July 6, 1970. Part of this paper was presented as Paper 68-701 at the AIAA Fluid and Plasma Dynamics Conference, Los Angeles, Calif., June 24–26, 1968. This work was accomplished under the sponsorship of the Advanced Research Projects Agency and was administered through SAMSO, Contracts AF-04-(694)-992, F04701-68-C-0041, and F04701-69-C-0119. This paper has benefited from the guidance and contributions of L. A. Hromas and the late W. H. Webb, especially in the comparison with the predictions of wake velocity, density, and scale.

* Member of the Technical Staff, Fluid Physics Department. Member AIAA.

† Member of the Technical Staff, Fluid Physics Department. Associate Member AIAA.

had identical configurations, i.e., both probes were either the hot-film or the cooled-film type and both probes had the same operating temperature. (Constant temperature or resistance type of anemometer electronics is used in this application.[16]) With this arrangement, the two probes had identical sensitivities to velocity and temperature. Cross-correlations between data from the closely spaced probes provided information about the structure of the velocity and temperature fluctuations. Orthogonal shadowgraphs were taken as shown in Fig. 1 to determine the probe-to-projectile axis distance, which was between one and two projectile radii. The anemometer data was recorded on a magnetic tape recorder and later digitized and processed on a digital computer.

Velocity measurements were obtained with two techniques, one using the average measurements and the other using the fluctuations. The first method utilized the calibration of the probes, both in an oven for temperature-resistance information and in a jet for velocity response measurements. The data closely approximated King's law, $q/\Delta T = A + B(U)^{1/2}$, where $q$ was the heat loss from the probe, $\Delta T$ was the temperature difference between the probe and the flow, and $U$ was the velocity, $A$ and $B$ being constants. During the experiment, the probes were operated at low temperature to emphasize the temperature effects in the data and at high temperature to emphasize the velocity effects. The highest probe temperature (450°C) was close to the limit for probe structural integrity, whereas the lowest temperature was close to the peak wake temperature being measured when hot-film probes were used. Hot-films, like hot-wires, must lose heat to the measured fluid. Cooled-film probes, on the other hand, can lose heat to an internal coolant and can thus operate at a lower temperature than the measured fluid. Probe temperatures as low as 70°C were obtainable in practice with cooled-film probes.

The digitized data was statistically processed on a computer using time segments that became longer as $X/D$ increased, according to the changing frequency content of the data. Each shot produced up to ten processed segments of the data per anemometer, each of which gave a mean value. At each of the ten $X/D$ locations there were two mean values per shot. At least four repeated shots, and most often five or more, were used to complete a set of data for averaging together at each $X/D$. This procedure was needed to get a sufficient range of statistical variation and thus, a meaningful average.[17] In physical terms, the averaging between shots was needed because of the relatively few turbulent configurations that appear at the probe before a significant change of the mean properties occurs. Additional shots give statistically independent samples out of the range of possible turbulent configurations at each $X/D$. The average between shots is thus a valid representation of the mean wake properties, being obtainable because of the modest cost per launch.

The anemometer data for each $X/D$ segment was averaged over the two anemometers per shot and over the several shots to give a mean value for each probe temperature. A new series of shots was used for each change in probe temperature. Two probe temperatures were sufficient to produce mean wake velocity and mean wake temperature, using the jet and oven calibrations. For the cases where velocity and temperature fluctuations were measured, a third set of data with an intermediate probe temperature was obtained. This data provided redundancy in mean velocity and temperature, thus increasing the accuracy of the measurements. To obtain the velocity and density fluctuations, the King's law calibration equation was resolved into mean and fluctuating components, squared, ordered, and averaged in a conventional manipulation of this equation.[18] The three unknowns $\langle U'^2\rangle$, $\langle U'T'\rangle$, and $\langle T'^2\rangle$ were obtained from the three sets of fluctuating data $\langle q'^2\rangle$ with varying sensitivities to each unknown. The $\langle q'^2\rangle$ values from each shot and

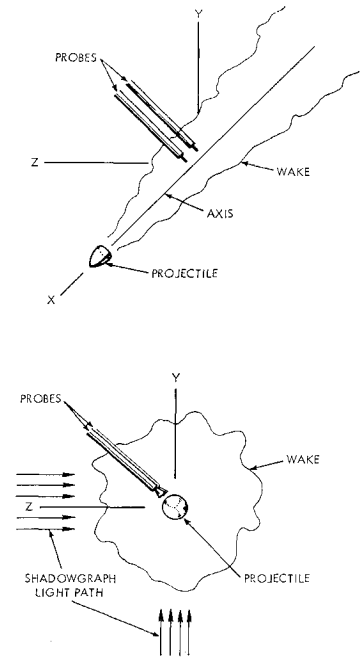


**Fig. 1 Configuration of the ballistic range experiment.**

anemometer were averaged across the two anemometers and several shots for fixed $X/D$, as before.

The second method of obtaining an average velocity, namely the convection velocity, utilized the average delay time for best cross correlation between the two anemometer probes. This delay time corresponded to the average time for a fluctuation of the turbulence to be convected from one probe to the other. This average time, divided into the probe spacing, produced the convection velocity.

The cross- and auto-correlation were calculated using the formulation,

$$C_{gh}(\Delta x, \Delta t) = \frac{\Sigma g(0,t)\ h(\Delta x, t + \Delta t)}{[\Sigma g(t)\ g(t)]^{1/2}\ [\Sigma h(\Delta x,t)\ h(\Delta x,t)]^{1/2}}$$

where $g$ and $h$ are the finely digitized data from the two anemometers, and $\Delta x$ and $\Delta t$ are probe separation and delay time, respectively. For the auto-correlation, $g = h$ and $\Delta x = 0$. These two correlations were also Fourier transformed into the power spectrum and cross spectrum, respectively. The required averaging time increased with $X/D$ because of the decreasing frequencies of the turbulent fluctuations. This feature of ballistic range data reduction was discussed by Fox.[16]

Both space and time scales of the turbulent fluctuations were calculated. The space scale was obtained from the simultaneous cross-correlation data ($\Delta t = 0$) for the one or two values of probe spacing $\Delta x$ that were used. The space correlation function was estimated from these data and then integrated to provide the space correlation length or scale $\Lambda$. The time correlation scale $\theta$ was obtained from the frequency equivalent of the auto-correlation integral[16] $\theta = P(0)/4R(0)$. Another estimate of $\Lambda$ was provided by Taylor's hypothesis, namely $\Lambda = \theta U_w$, where the predicted $U_w$ was used. Good agreement was obtained between these two methods and the LHW prediction of $\Lambda$.

## 3. Velocity Results

The mean wake velocity results behind a sphere projectile at 6000 fps (Fig. 2) were obtained with three probe temperatures, 445°, 255°, and 70°C. Hot-film probes were used for the 445° and 255°C measurement, and cooled-film probes were used for the 70°C measurements. Because the mean

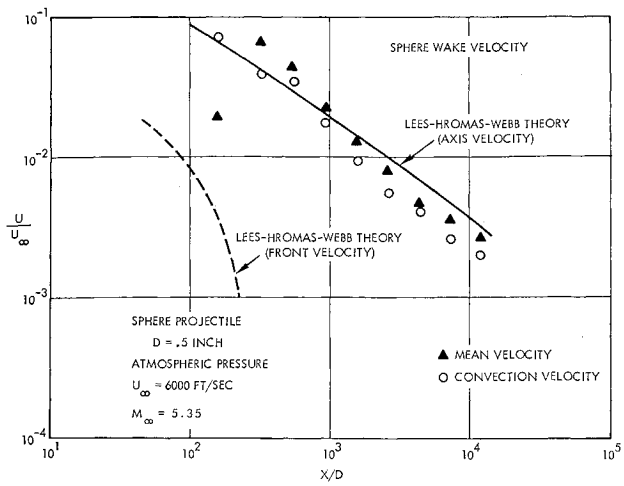


**Fig. 2 Hot- and cooled-film anemometer measurements of sphere-wake axis velocity compared with predictions from Lees-Hromas-Webb Theory. Off-axis effects are noticeable at low $X/D$.**

velocity and temperature can be deduced from just two probe temperatures, as outlined in the previous section, the wake properties were obtained both with and without the cooled-film anemometer probes. The agreement between the two methods became a verification of the cooled-film anemometer, which is a relatively new instrument. Results from the two methods and the two separate anemometers, which varied only randomly from each other, were averaged together to increase the statistical reliability or accuracy of the result.

The mean velocity results can be compared with the Lees-Hromas-Webb prediction, which is shown in Fig. 2 as axis velocity and front velocity. The turbulent front has a finite velocity in hypersonic wakes at low $X/D$ because of the bow shock drag that is deposited inviscidly outside the turbulent core. As this outer drag is engulfed by the turbulence, the front velocity drops, as is shown in Fig. 2 at 250 diam.

The first mean velocity data are taken shortly after the probe is engulfed by the wake but still located significantly off-axis at $X/D = 160$. (Values are plotted at the midpoint of the segment of raw data used for reduction.) As $X/D$ increases, the wake grows and the off-axis effect on the data rapidly decreases to a few percent. Good agreement with the LHW prediction of axis velocity is achieved. Asymptotic slopes of $X^{-2/3}$ are achieved by both the data and the LHW calculation. This final slope is one of the fundamental features of the LHW theory resulting from the theoretical transformation of low-speed wakes into hypersonic wakes.

It is worth mentioning, before the discussion in the following section, that the mean velocity and temperature measurements have been checked by calculating total wake enthalpy. This quantity should be essentially constantly at the downstream wake stations sampled as a result of prior turbulent entrainment. A check of the measurements was obtained within a random $\pm$ 20% variation except at the first location, $X/D = 160$, where 50% was obtained. For ballistic range measurements, this accuracy is considered very good.

Convection velocity measurements, which were obtained from the delay time for best cross-correlation, are also shown in Fig. 2 for the sphere wakes. Included in the average data are data from all 15 shots.

The convection velocity is initially greater than the mean velocity, when the probe is near the edge of the wake ($X/D = 160$). This phenomenon is similar to that observed at the edge of jets.[19] The turbulent eddies at the edge of a wake or jet appear infrequently and intermittently, but they have high velocity compared with the laminar fluid. Thus the convection velocity, which measures the turbulent velocity, is higher than the mean velocity, which measures both laminar and turbulent parts of the flow.

Comparison with LHW calculations and other measurements is shown in Fig. 3 where the drag length $(C_DA)^{1/2}$ has been used to normalize wake distance. This length will cause the velocity $U/U_\infty$ to coincide with a slope of $X^{-2/3}$ at large $X/(C_DA)^{1/2}$ for all Mach numbers and projectile shapes, as discussed in Refs. 6 and 7. The intermediate slope of $X^{-1}$ in axis velocity predicted at $M_\infty = 22$ occurs just after the wake has swallowed all the inviscid drag. Under these extreme density ratio conditions at intermediate $X/(C_DA)^{1/2}$, the turbulent wake grows rapidly in diameter, simultaneously slowing down more rapidly than the final $X^{-2/3}$ trend. This $X^{-1}$ slope in axis velocity can be demonstrated as a limiting case of the theory of Refs. 3–7 at high Mach numbers. At low Mach numbers, less of this appears, as shown in Fig. 3.

The measurements of sphere wake velocity shown in Fig. 3 include electrostatic probe and sequential spark measurements,[1,2] sequential schlieren measurements,[8] as well as the present anemometer measurements. The sequential spark and electrostatic probe measurements are effective in the middle range of $X/(C_DA)^{1/2}$; they overlap the new anemometer data that extend to the far range of $10^4$ in $X/(C_DA)^{1/2}$. All these data verify the predicted axis velocity of the LHW calculations at high Mach number. The asymptotic trend of $X^{-2/3}$ is clearly shown only by the anemometer data among the local measurements.[1,2] It is noteworthy that integrated measurements with the sequential schlieren[8] produce lower values than the local measurements as well as an asymptotic slope of $X^{-2/3}$.

Cone-wake velocity is shown in Fig. 4. The predictions of axis and front velocity provided by the LHW theory are shown for the case of a high Mach number wake. Only small changes were obtained for the $M = 6$ case that was calculated; these changes are omitted from Fig. 4. The front velocity shows the flatter distribution of inviscid drag that occurs behind a cone projectile as compared with that behind the spheres of Fig. 2 and 3. The asymptotic decay of the cone axis velocity coincides with the final sphere wake velocity of Figs. 2 and 3.

The anemometer measurements behind sabot-launched spinning slender cones at 6 kfps were obtained with the convection velocity technique of cross-correlating the fluctuations. The lowered anemometer power level at this low range pressure of 100 torr permitted just the high probe temperature to be used with the hot-film probes. Five shots were used for data reduction and averaging. The off-axis position of the probes ranged up to two projectile diameters. The agreement between the LHW prediction is good and well within the precision of the data.

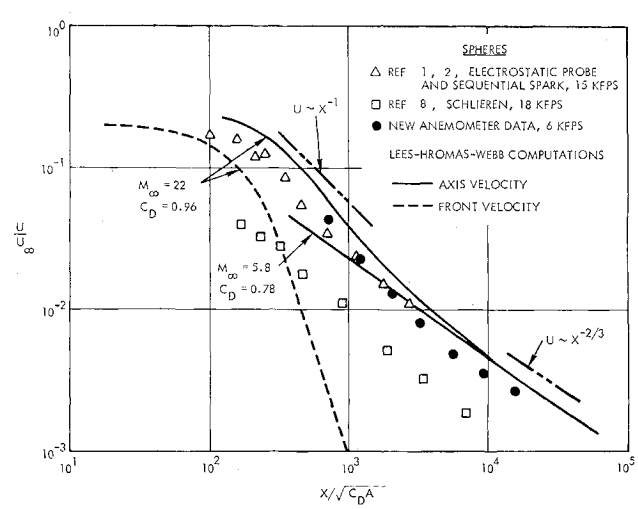


**Fig. 3 Sphere wake axis velocity measurements compared with Lees-Hromas-Webb computations.**

Schlieren velocity data[8] for slender cone wakes are also shown in Fig. 4. Some off-axis sensitivity seems to influence these results because of the lower trend compared with the anemometer data and the LHW prediction. This effect is smaller for cones than for spheres using the same schlieren technique (see Fig. 3).

Earlier anemometer measurements of 0.22 caliber blunt bullet wakes at 4 kfps are shown in Fig. 5. Excellent agreement is shown between the mean wake velocity measurements and the LHW computations. The high Mach number wake computation for blunt bodies in Fig. 5 shows some of the $X^{-1}$ slope in axis velocity that occurs for sphere wakes, as shown in Fig. 3. Hot-film anemometer temperatures of 62°, 166°, and 270°C were used. Probe-to-projectile axis distances of about one projectile diameter were obtained.

The wake temperature measurements $T$ that were simultaneously obtained with the anemometer velocity measurements are also shown in Fig. 5. The normalization as

$$(T/T_\infty - 1)\ [M_\infty^2(\gamma_\infty - 1)]^{-1}$$

is indicated by the energy equation of fluid mechanics. The degree of agreement between the temperature and velocity results in Fig. 5 shows the degree of consistency with the conservation of total enthalpy; perfect agreement would indicate perfect measurements. Up to 40% disagreement is shown in Fig. 5. Considerably better agreement is obtained with the more recent sphere measurements of velocity and temperature, as previously discussed. The LHW computations show the agreement between predicted velocity and temperature in Fig. 5 for the blunt bullet wake; the two curves coincide except for a small separation between them at $X/(C_DA)^{1/2}$ less than 200. The details of the comparison between wake velocity and temperature will be discussed in the next section.

From Ref. 20, the wake velocity behind a slender rod in a wind tunnel at $M = 3$ is also shown in Fig. 5. The rod extended from the stagnation chamber through the throat of the tunnel and terminated in the test section. No significant shock waves appeared in the test flowfield; the entire drag was embodied in the thick laminar boundary layer and viscous wake, which became turbulent several diameters behind the rod. These details of the flow are important when attempting a comparison with projectile wakes, which contain a major portion of the drag in an inviscid flow caused by the bow shock wave. The slender rod wake starts out in the same general range of $U/U_\infty$ as the blunt bullet prediction, but it quickly assumes the asymptotic slope of $X^{-2/3}$. (This slope is

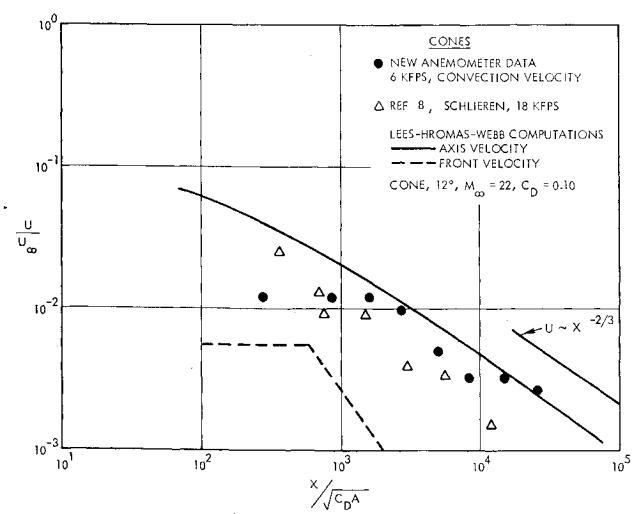


**Fig. 4 Anemometer measurements of cone-wake axis velocity compared with schlieren measurements and Lees-Hromas-Webb computations. Off-axis effects are noticeable at low $X/D$.**

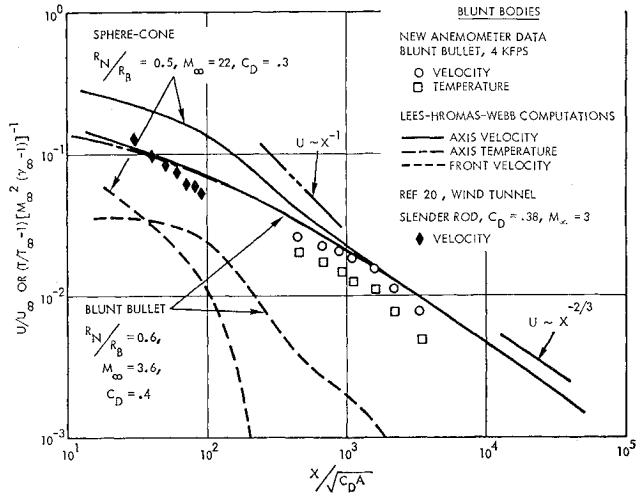


**Fig. 5 Axis velocity and temperature measurements of blunt-body wakes using anemometers compared with Lees-Hromas-Webb computations and wind tunnel measurements.**

shown more convincingly in Ref. 20.) This feature is consistent with the lack of inviscid drag. Perhaps the best way to compare the rod and projectile wakes is to consider the rod wake to have a shorter starting length $X_0$. Then the final trend $(X - X_0)^{-2/3}$ appears logically at a smaller $X/(C_DA)^{1/2}$ in Fig. 5 for the rod than for the projectiles. Within this concept, the projectiles have the starting length $X_0$ extended because of the inviscid wake.

## 4. Density Results

It is worth discussing certain unfamiliar aspects of the compressible flow energy equation that were alluded to in the previous discussion. The conservation of total enthalpy in body-fixed coordinates takes the form

$$U/U_\infty - U^2/2U_\infty^2 = [1/M_\infty^2(\gamma_\infty - 1)]\ [h/h_\infty - 1] \quad (1)$$

when the wake velocity $U$ is given in "ballistic range" coordinates, *i.e.*, fixed with respect to the undisturbed freestream. (The Prandtl number effect, which is at most 13% in the wake core is neglected compared with the attainable accuracy of ±20%.) For the wake calculations and data shown here, the second term is at most 15% of the first term and is completely negligible when $U/U_\infty$ is less than 0.1. Thus to a good approximation, the second term can be discarded in favor of the first term. When $M_\infty$ is not too high, constant $c_p$ can be taken in the wake, and Eq. (1) becomes

$$U/U_\infty \approx [1/M_\infty^2(\gamma_\infty - 1)]\ [T/T_\infty - 1] \quad (2)$$

The approximation becomes an equality at large $X/(C_DA)^{1/2}$. At distances greater than $X/(C_DA)^{1/2} = 80$, sphere wakes are at freestream pressure. [Freestream pressure occurs at lesser $X/(C_DA)^{1/2}$ for blunt bodies and cones.] Thus, $T/T_\infty = \rho_\infty/\rho$, within the fixed gas constant $R$ restriction. In summary, the approximation

$$\frac{U}{U_\infty} \approx \frac{1}{M_\infty^2(\gamma_\infty - 1)}\left[\frac{T}{T_\infty} - 1\right] \approx \frac{1}{M_\infty^2(\gamma_\infty - 1)}\left[\frac{\rho_\infty}{\rho} - 1\right] \quad (3)$$

approaches an equality for $U/U_\infty < 0.1$, for $X/(C_DA)^{1/2} > 80$, or for $X/(C_DA)^{1/2}$ greater than a certain value, depending on $M_\infty$, such that constant $c_p$ and $R$ may be used.

It is evident that Eq. (3) provides a basis for comparison of $T$ and $\rho$ measured at various $M_\infty$. In Fig. 6, several measurements of sphere wakes are shown along with the anemometer results and the LHW predictions. The LHW predictions of

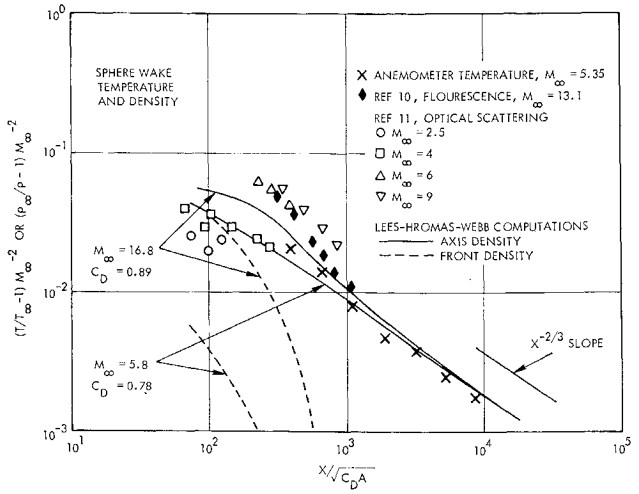


**Fig. 6 Axis sphere wake temperature measurements using anemometers compared with Lees-Hromas-Webb computations and optical density measurements.**

$T$ and $\rho$ show the same general trend and same $X^{-2/3}$ asymptotic slope as that shown in Fig. 3 for the velocity of sphere wakes at high and moderate $M_\infty$. Indeed, Eq. (3) states that this similarity must exist. The LHW predictions in Fig. 6 show less change with $M_\infty$ at low $X/(C_DA)^{1/2}$ than those in Fig. 3; the influence of $c_p$ and $R$ variation in Fig. 6 causes this difference. It should be noted that when $U$, $T$, and $\rho$ are plotted as indicated in Eq. (3), they will coalesce and take the $X^{-2/3}$ slope at large $X/(C_DA)^{1/2}$ for all projectile slopes and all $M_\infty$.

The anemometer measurements in Fig. 6 agree with the LHW prediction and provide the $X^{-2/3}$ slope at large $X/(C_DA)^{1/2}$. As previously remarked, the anemometer data gives both $U$ and $T$. Thus, total enthalpy conservation provides a test for the internal consistency of the data. The data passed this check within 20% for all the data shown in Fig. 6. It is noteworthy that this test is one of the few fundamental checks using the basic equations of compressible flow that are available to ballistic range measurements. Moreover, anemometers are unique in providing all the necessary measurements, namely $U$ and $T$, from a single instrument to provide such a fundamental check.

The fluorescence measurements of $\rho$ were provided by electron-beam excitation of nitrogen, at range pressures up to 7.6 torr using a 2.7-in. diam projectile.[10] The data provide somewhat lower density (higher $\rho_\infty/\rho$) at low $X/(C_DA)^{1/2}$ than the LHW prediction, but they agree with the prediction at larger $X/(C_DA)^{1/2}$.

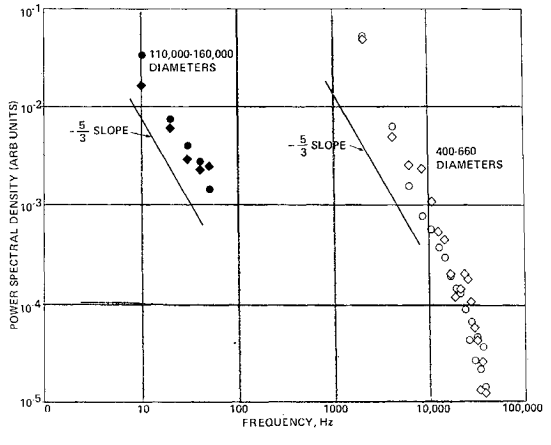


**Fig. 7 Typical power spectral densities for small and large $X/D$ compared with Kolmogoroff slope.**

The density measurements of Ref. 11 shows less agreement with the LHW prediction and also show a stronger $M_\infty$ dependence of $\rho_\infty/\rho$ than the prediction. This experiment was conducted using the intensity of Rayleigh scattering of laser light from the molecules of the wake flow, as measured remotely by an optical system and photomultiplier. The range pressure was atmospheric, and possible random refractions of the scattered light from the turbulent wake may have led to measurement error.

Fluctuation intensity measurements of $\langle U'^2\rangle^{1/2}/U, \langle T'^2\rangle^{1/2}/T - T_\infty$, and $\langle \rho'^2\rangle^{1/2}/\rho - \rho_\infty$ were made with the three-probe-temperature method. Sphere wake measurements of these quantities were near 0.2, and blunt bullet wake measurements were near 0.4. These measurements are regarded as preliminary, but they are within the range of expected values from earlier measurements at low $M_\infty$.[12-14]

## 5. Spectra and Time Correlation Results

Each of the segments of raw data from the anemometers were spectrally analyzed on a digital computer. The auto- and cross-correlations and their Fourier transforms, the power and cross-spectra, were calculated. Typical of the range of spectra or frequency distributions of the fluctuations that were produced are those shown in Fig. 7, where there is also shown the Kolmogoroff slope of $-\frac{5}{3}$ for comparison. The two symbols for the spectrum refer to simultaneous data from the two anemometers. Each of the analyzed segments of data had its auto- and cross-spectrum examined before it was accepted for averaging with data from other shots. A reasonably smooth spectral distribution was required as well as a dynamic range at least as good as the 110,000–160,000 diam examples in Fig. 7. Further results were concerned with integral measures of spectra, such as time correlation integral scale and space correlation length scale.

The time correlation integral scale is defined as the integral of the autocorrelation function. For ballistic range data this scale is better calculated from the zero frequency intercept of the spectrum, as discussed in Ref. 16. The time correlation scale is defined as an average time to randomness[18] or a typical inverse frequency in the spectrum. It is not surprising, therefore, to find in Fig. 8 that the time correlation scale $\theta$ is small at $X/D = 500$ where the turbulent fluctuations are at high frequencies as shown in Fig. 7. Conversely, a large $\theta$ can be expected at $X/D = 130{,}000$ where the turbulent frequencies are low. In Fig. 8 the range of cone and blunt body data are shown as $\theta\, U_\infty/D$. The two time correlation scales for cones and blunt bodies agree with each other and with the line $\theta \sim X$. This trend will take on significance when Taylor's hypothesis is later used to compare the time correlation scale $\theta$ with the space correlation length scale $\Lambda$.

The average between shots and anemometers is shown in Fig. 9 for the sphere wakes. The three probe temperature measurements are shown to agree with the cone and blunt bullet data at $X/D$ larger than 2500 when the data are nor-

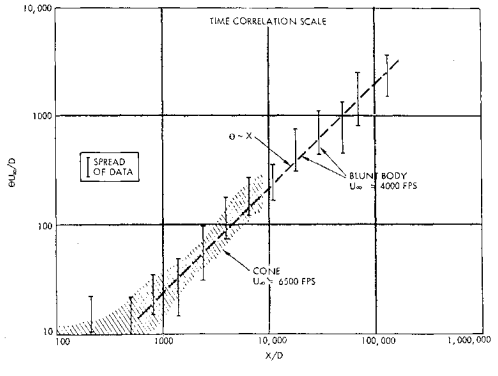


**Fig. 8 Time correlation integral scale measurements.**

malized as $\theta\, U_\infty/D$. At $X/D$ less than 2500, the values of $\theta$ for the sphere wake are separated according to the values of $\Delta T$, the temperature difference between the probe and the wake. The physical significance of low or high $\Delta T$ is the degree of sensitivity of the anemometer data to velocity or temperature fluctuations. At low $\Delta T$, the anemometer acts more like a thermometer, and the data fluctuations are mainly temperature fluctuations. At large $\Delta T$, the velocity fluctuations contribute significantly to the anemometer data. In Fig. 9, at low $X/D$, the temperature sensitive data are shown to produce larger values of time correlation scale $\theta$ than the velocity sensitive data. Thus, the temperature fluctuations have lower frequency content than the velocity fluctuations.

## 6. Space Correlation Length

In Fig. 10 are shown the measurements of space correlation length scale $\Lambda$ for the cone and blunt bullet wakes along with the LHW predictions for these cases. The scaling of $\Lambda$ with $M_\infty{}^{2/3}\,(C_DA)^{1/2}$ comes from the use of the enthalpy width as the significant length for $\Lambda$.[5] At large $X/(C_DA)^{1/2}$, the correlation length predictions agree for the two bodies, and they approach the $X^{1/3}$ trend that is found in low-speed wakes. The measurements of $\Lambda$ for both the cone and blunt bullet wakes agree with the LHW predictions and also agree with each other. A reasonably large variation of $M_\infty$ and $(C_DA)^{1/2}$ was obtained with the two measurements so that a good test of the scaling was obtained.

The measurements of $\Lambda$ were obtained using simultaneous cross-correlation of the data from the two anemometers. As defined, $\Lambda$ is a measure of an average eddy size or average fluctuation size. The simultaneous cross-correlation measures how well the fluctuations are correlated at a given probe spacing $\Delta X$. A very small spacing $\Delta X$ gives a perfect correlation value of unity, and a very large spacing $\Delta X$ gives zero correlation. The integral of this space correlation function for all $\Delta X$ is defined as $\Lambda$. Estimates of this function were obtained from one or two probe spacings. Blunt bullet wakes were measured with spacings $\Delta X$ of $D/2$ and $D$, using 10–15 shots for averaging. For the cone data, a single spacing $\Delta X = D/2$ was used with 7 shots for averaging. The estimated correlation function was composed of straight lines passing through the measured average correlation values together with a value of unity at $\Delta X = 0$, as provided by definition. Long tails were thus avoided in the estimated correlation function, the integral of which was the estimate of $\Lambda$, shown in Fig. 10. This method was tested for the various shapes of correlation functions that have been measured,[18] and it was found to reproduce the integral value of $\Lambda$ within

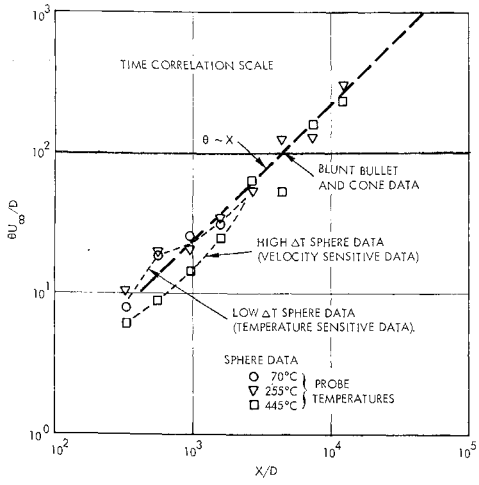


**Fig. 9 Time correlation integral scale for the sphere wakes.**

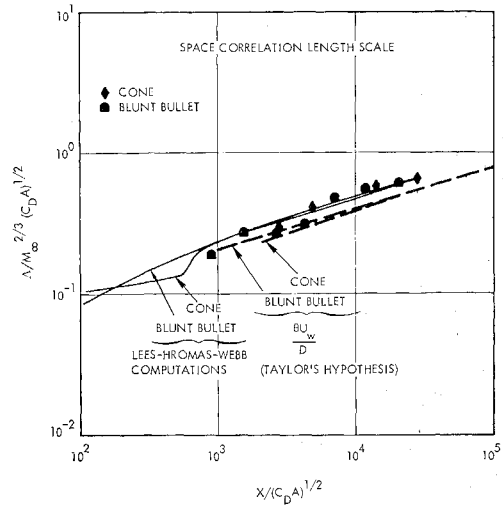


**Fig. 10 Space correlation length scale for the cone and blunt bullet wakes compared with the Lees-Hromas-Webb computations.**

about 50% for most of the expected shapes. This limit controlled the over-all precision of the method because the shot-to-shot averaging of the correlation measurements had greater stability. The excellent agreement of the cross-correlation $\Lambda$ with the LHW prediction is verified by the results of the Taylor's hypothesis method of measuring $\Lambda = \theta U$, which are also shown in Fig. 10. The Taylor's hypothesis method has greater over-all precision, being based on the notion of frozen turbulence.[18] The turbulence is not actually frozen as it passes over a fixed probe, but rather the time scale for change of turbulence is much larger than the time of passage over the probe. Within this concept, $\theta U$ is equivalent to $\Lambda$. Both $\Lambda$ and $\theta U$, the predicted $U$ being used, attain the asymptotic trend of $X^{1/3}$. The trend of $\theta \sim X$ can be seen in Fig. 8 and $U \sim X^{-2/3}$ in Figs. 3 and 4; the asymptotic trend of $\theta U \sim X^{1/3}$ follows logically.

The cone and blunt bullet measurements of $\Lambda$ and $\theta$ showed no sensitivity to the probe temperature. This insensitivity implies that the temperature and velocity fluctuations have the same structure within the precision of the experiment. For the sphere wake measurements of $\Lambda$ shown in Fig. 11, a quite different situation is shown for $X/(C_DA)^{1/2}$ less than 2500. The low $\Delta T$ measurements, that is, those most sensitive to temperature fluctuations, have a larger $\Lambda$ or fluctuation size. Conversely, the high $\Delta T$ measurements, being sensitive to

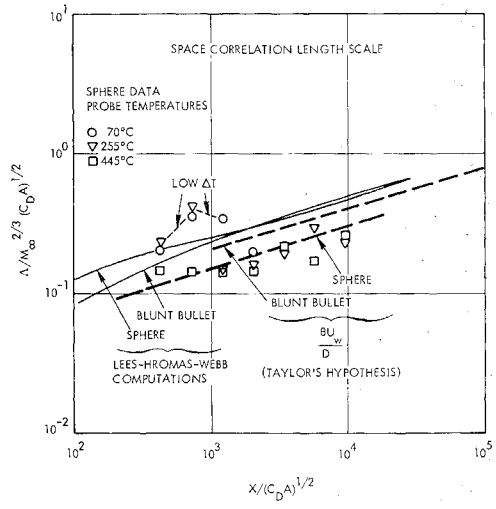


**Fig. 11 Space correlation length scale for the sphere wakes compared with the Lees-Hromas-Webb computations.**

velocity fluctuations, show a smaller $\Lambda$. (A single probe spacing of $D/2$ was used for the sphere measurements.) These measurements of $\Lambda$ are consistent with the $\theta$ measurements shown in Fig. 9. The temperature fluctuation eddies are larger and, logically, slower in fluctuations; that is, $\theta$ is larger and fluctuation frequencies are lower. Conversely, the velocity eddies are smaller and have higher frequencies.

This double structure of large temperature scale and small velocity scale evidently arises from the large temperature and velocity difference between the axis and front location of the wake. The sphere wakes provide larger values than those measured in the cone and blunt-body wakes. It is worth noting that the convection velocity measurements of the sphere wakes, which utilize the delay-time feature of the fluctuations, show no sensitivity to $\Delta T$. Thus, the temperature fluctuations are larger and have lower frequency than the velocity fluctuations, but they move with the same average velocity as the velocity fluctuations.

For $X/D$ greater than 2500, the various anemometer probe temperatures produce the same $\Lambda$, the value of $\Lambda$ being lower than expected; agreement between $\Lambda$ and $\theta U$ was obtained, nevertheless.

## 7. Conclusions

Projectile wake velocity, density, and temperature have been measured for spheres, cones, and blunt bullets using anemometers. Excellent agreement with the Lees-Hromas-Webb computations was obtained including the $X^{-2/3}$ asymptotic trends. In comparisons with other results, good agreement was obtained with probe measurements, but less agreement was obtained with optical methods. Comparison with a slender rod wake in a wind tunnel was limited because of the lack of an inviscid wake in that flow. Measurements of time and space correlations in cone and blunt bullet wakes showed agreement with the LHW predictions. Evidence of a double structure of the turbulence in sphere wakes at low $X/D$ was found, i.e., the temperature fluctuation eddies were larger and at lower frequency than the velocity fluctuation eddies.

## References

[1] Heckman, D. et al., "Convection Velocity Measurements in Hypersonic Sphere Wakes," *AIAA Journal*, Vol. 6, No. 4, April 1968, pp. 750–752.

[2] Lahaye, C., Leger, E. G., and Lemay, A., "Radial and Axial Velocity Profiles of Hypersonic and Supersonic Wakes Measured by the Sequential Spark Method," *AGARD Conference Proceedings*, No. 19, Fluid Physics of Hypersonic Wakes Conference, Fort Collins, Colo., May 1967.

[3] Lees, L. and Hromas, L., "Turbulent Diffusion in the Wake of a Blunt Body at Hypersonic Speeds," Rept. 6110-005-MU000, July 1961, TRW Space Technology Labs.; also *Journal of the Aerospace Sciences*, Vol. 29, 1962, pp. 976–993.

[4] Webb, W. H. and Hromas, L., "Turbulent Diffusion of a Reacting Wake," *AIAA Journal*, Vol. 3, No. 5, May 1965, pp. 826–837.

[5] Webb, W. H., "A Model for the Calculation of Radar Backscatter from Underdense Hypersonic Turbulent Wakes," Rept. 6433-6005-KU000, June 8, 1964, TRW Space Technology Labs.; also "Self-Preserving Fluctuations and Scales for the Hypersonic Turbulent Wake," *AIAA Journal*, Vol. 2, No. 11, Nov. 1964, pp. 2031–2033.

[6] Hromas, L. A. and Lees, L., "Effect of Nose Bluntness on the Turbulent Hypersonic Wake," Rept. 6130-6259-KU000, Oct. 1962, TRW Space Technology Labs., Redondo Beach, Calif.

[7] Lees, L., "Hypersonic Wakes and Trails," Paper 2662-62, ARS 17th Annual Meeting, Nov. 1962; also *AIAA Journal*, Vol. 2, No. 3, March 1964, p. 417–428.

[8] Herrman, J., Slattery, R. E., and Clay, W. G., "Measured Properties of the Wakes of Hypersonic Cones," AIAA Paper 68-687, Los Angeles, Calif., 1968.

[9] Lien, H. and Eckerman, J., "Interferometric Analysis of Density Fluctuations in Hypersonic Turbulent Wakes," *AIAA Journal*, Vol. 4, No. 11, Nov. 1966, pp. 1988–1994.

[10] Tardiff, L. and Dionne, J. G. G., "Density Distribution in Turbulent and Laminar Wakes," *AIAA Journal*, Vol. 6, No. 10, Oct. 1968, pp. 2027–2029; also CARDE TN 1830/69, April 1969, Canadian Armament Research and Development Establishment, Valcartier, Quebec.

[11] Locke, E., "Point Measurements of Time-Averaged Turbulent Wake Density by Rayleigh Scattering," *AIAA Journal*, Vol. 5, No. 10, Oct. 1967, pp. 1888–1890.

[12] Townsend, A. A., *The Structure of Turbulent Shear Flow*, Cambridge U. Press, Cambridge, England, 1956, Chap. 7.

[13] Demetriades, A., "Turbulence Measurements in an Axisymmetric Compressible Wake," *The Physics of Fluids*, Vol. 11, No. 9, Sept. 1968, pp. 1841–1852.

[14] Gibson, C. H., Chen, C. C., and Lin, S. C., "Measurements of Turbulent Velocity and Temperature Fluctuations in the Wake of a Sphere," *AIAA Journal*, Vol. 6, No. 4, April 1968, pp. 642–649.

[15] Fox, J. et al., "Hot-Wire Measurements of Wake Turbulence in a Ballistic Range," *AIAA Journal*, Vol. 5, No. 1, Jan. 1967, pp. 99–102.

[16] Fox, J., "Space Correlation Measurements in the Fluctuating Turbulent Wakes Behind Projectiles," *AIAA Journal*, Vol. 6, No. 2, Feb. 1968, pp. 233–238; Rept. 07854-6021-R000, Feb. 1967, TRW Systems Group, Redondo Beach, Calif.

[17] Blackman, R. B. and Tukey, J. W., *The Measurement of Power Spectra*, Dover, New York, 1959.

[18] Hinze, J. O., *Turbulence*, McGraw-Hill, New York, 1959.

[19] Davies, P. O. A. L., "Turbulent Structure in Free Shear Layers," *AIAA Journal*, Vol. 4, No. 11, Nov. 1966, pp. 1971–1978.

[20] Demetriades, A., "Mean Flow Measurements in an Axisymmetric Compressible Turbulent Wake," *AIAA Journal*, Vol. 6, No. 3, March 1968, pp. 432–439.